This article has been accepted for publication in IEEE/ACM Transactions on Audio, Speech and Language Processing. This is the author's version which has not been fully edited and content may change prior to final publication. Citation information: DOI 10.1109/TASLP.2024.3350882

A Parallel Analog and Digital Adaptive Feedforward Controller for Active Noise Control

Yoav Vered and Stephen Elliott

***Abstract*—Digital adaptive controllers are widely used for feedforward active noise control, especially in headphones. In such applications, the secondary path delay, including the sampling and reconstruction effects, must be shorter than the primary path delay to maintain good broadband performance. A mixed analog and digital adaptive feedforward controller is developed to eliminate the added delay of the sampling and reconstruction. The analog controller is based on a state-filtered adaptive linear combiner, while the digital one uses an adaptive finite-impulse-response filter. It is shown that both filters can be adapted using the normalized filtered-reference LMS algorithm but with different secondary paths' models. A method to design the analog state-filter based on Padé's approximation is described. The performance of the proposed controller with two analog states, the direct feedthrough and a 0.3 milliseconds delay, is assessed and compared to the separate analog or digital controllers in a controlled environment. The results highlight that adding the analog delay improves the digital controller performance by about 5 dB in this application, regardless of the primary noise direction.**

***Index Terms*—Active noise control, adaptive control, hybrid control, Padé approximation.**

I. Introduction

ACTIVE noise control (ANC) is used extensively to reduce undesired noise in headphones. Typically the controller is designed with two degrees of freedom [1]–[3]. A feedforward controller, usually in the form of a finite impulse response (FIR) filter, and a feedback controller, which is generally analog with a low-order infinite impulse response. The feedforward FIR filter's coefficients, or weights, are usually adjusted in real-time to adapt to the changes in the environment. The filtered-reference least-mean-squares (FxLMS) [4]–[6] algorithm is, probably, the most widely-used algorithm for the filter direct adaptation. The FxLMS is derived for the sampled-time domain and traditionally is realized on a digital signal processor (DSP) [7], [8], but it can also be realized on a microcontroller [9], [10] or VLSI implemented on a field-programmable logic array (FPGA) [11]–[13]. Assuming that no aliasing occurs, that the different systems are all linear and time-invariant (LTI), and that the reference signal is stationary in time, the FxLMS algorithm, if stable, converges to the optimal Wiener filter [6]. Anti-aliasing and reconstruction filters, and analog-to-digital (ADC) and digital-to-analog (DAC) converters are used to sample the reference and error signals and excite the speaker with the control signal. The different filters and the signal sampling introduce a time delay to the controller action, such that the controller's latency is increased, and as a result, the attainable attenuation levels are reduced [14]–[16].

Numerous methods and algorithms have been proposed to reduce the controller's latency [17]. These approaches can be divided into ones that use a single, high, sample rate [18], those that use a decimation [19], and those that use a multi-rate approach with digital decimation and interpolation filters [17] in addition to the analog anti-aliasing and reconstruction filters. However, even when a fast FPGA is used with these approaches, the latency does not vanish completely. Moreover, when a high sample rate is used, and the filter's impulse response is required to act over a given period of time, the computation of the control signal requires processing power proportional to the square of the sampling frequency and is prone to numerical ill-conditioning and misadjustment [17]. Both the requirement to reduce the latency and to allow for long impulse response can be maintained by using multi-rate methods when tuned correctly. However, the base sample rate needs to be sufficiently large, and several levels of decimations and interpolations are needed, in most applications, to enable the implementation of the digital low-pass filters required for the digital decimation and interpolation.

The idea of an all-analog (continuous-time) adaptive filter was originally used in the motivation for deriving the FxLMS [4], [5], [20]. The adaptable analog filter is usually portrayed as a linear combiner with adjustable weights (gains), where each signal is obtained either by using a delay element or a state-filter. However, since the introduction of the DSP, these methods have been forsaken due to the ease of implementation of an all-digital adaptive controller. This progression from analog to digital controllers is attributed both to the fact that the implementation of the adaptation law using analog integrator becomes complex for large filters and the difficulty of filtering the reference with an analog model of the secondary path.

Some Ideas of using a digital controller to adapt an analog component have previously been discussed. One approach is to use the digital controller only for the adaptation [21] of the gains of the analog filter's states. However, since the analog filters' impulse responses are fixed, this approach introduces constraints on the obtainable FIR structure impulse response. Parallel analog and digital controllers have also been suggested in the past, which allow more freedom in the obtainable impulse response of the filter. Stothers and Scott [22] have proposed an adaptable analog feedthrough element controlled by a DSP in parallel to the adaptable digital controller that is

Institute of Sound and Vibration Research, University of Southampton, United Kingdom.
Emails: [v.yoav,s.j.elliott]@soton.ac.uk
This work was supported by the UK Engineering and Physical Sciences Research Council (EPSRC) through the DigiTwin project (grant EP/R006768/1)
Manuscript received July xx, 2023

Authorized licensed use limited to: UNIVERSITY OF SOUTHAMPTON. Downloaded on January 10,2024 at 08:26:16 UTC from IEEE Xplore. Restrictions apply.
© 2024 IEEE. Personal use is permitted, but republication/redistribution requires IEEE permission. See https://www.ieee.org/publications/rights/index.html for more information.

This article has been accepted for publication in IEEE/ACM Transactions on Audio, Speech and Language Processing. This is the author's version which has not been fully edited and content may change prior to final publication. Citation information: DOI 10.1109/TASLP.2024.3350882

also implemented on the same DSP. Tinker [23] has proposed to introduce an analog feedforward circuit in parallel to the digital feedforward controller, with an adaptable gain.

In adaptive signal-processing methods that are based on an adaptable analog filtering and the continuous-time LMS algorithm, the analog states are obtained by using all-pass filters [24], low-pass filters [25], adaptable state-space filter [26], or other approaches, see [27] and the reference therein. When all-pass filters are used, they have been classically designed using Laguerre or Kautz filters, whose group delay approximation is valid only at a small frequency bandwidth, compared to the Padé or Equiripple approximations [28].

In this work, a parallel analog and digital adaptive feedforward (ADAF) controller is introduced. The parallel adaptable analog filter enables the elimination of the controller's latency by realizing the initial transient response, while the digital filter is used to obtain good attenuation for realistic decay rates by realizing the later transient response of the controller's impulse response.

The novelty of the proposed controller is the fact that it enables the digital adaptation of several gains for the analog filter in real-time using the digital controller. This is achieved with different secondary path models for the analog and digital paths. The analog controller is designed using a 2nd order Padé approximation, which has larger frequency bandwidth compared to the same-order Laguerre approximation but can still be readily designed using an RC-opamp circuit, unlike the Equiripple approximation. These filters do not aim to obtain specific IIR responses but to approximate delay elements. The output of each state filter is passed through adaptable gain elements, and then all the analog states and the digital filtered control signals are summed to obtain the control signal that excites the speaker.

The ADAF controller structure is based on a conference proceeding [29] previously published by the authors. Although this only includes a simulative study comparing two possible structures for the analog delay tap for a pure delay scenario with no additional dynamics. It was found in [29], based on the simulations, that it is preferred to use a parallel approach to the analog filter over a series design, and this is adopted here. But now, a detailed analysis of the algorithm is discussed together with its real-time implementation and an experimental study of its performance.

The paper is organized as follows: Section II presents the system used for the case-study in Section II-A, the ADAF controller structure is shown in Section II-B, and the analytical derivation of the adaptation law for the digital and analog filters are derived in Sections II-B1 and II-B2, respectively. Section III presents the real-time experimental results. The design of the analog filters is described in Section III-A, then the results of the impulse response estimation experiments are shown in Section III-B, and finally, the experimental results of the ADAF varification experiments done in the anechoic chamber are reported in Sections III-C and III-D. The discussion and conclusions drawn based on the experimental results are reported in Section IV.

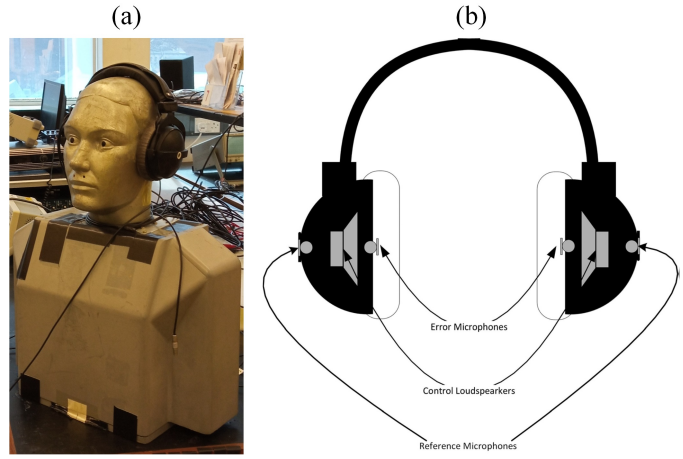

Fig. 1. Photo (a) and model (b) of the customized headphones.

II. Paraller analog and digital adaptive feedforward controller for active noise control for single-channel applications

This section will first describe the system used for the case study of the proposed parallel ADAF controller, and then the algorithms used for the implementation of the single-channel ADAF are derived.

A. System description

Figure 1 shows the customized headphones and the speaker and microphone configuration that are used in this work. A Beyerdynamic DT 770 Pro headphones are used, which were integrated with both reference microphones and error microphones in the shell of the ear cups and inside the ear cups, respectively, as shown in Figure 1(b). All microphones were omnidirectional electrets. To not over-complicate the ADAF derivation, only a single channel is considered here, namely that of the left ear cup of the headphones, shown in Figure 1(a). However, a similar algorithm can be readily derived for a multichannel system on the basis of the 2 by 2 algorithm proposed in [30].

B. Parallel controller structure

Figure 2 shows the proposed block diagram of the ADAF controller. In the block diagram, continuous signals are denoted as (t), sampled signals by $[n]$, and filtered signals are denoted with an apostrophe to distinguish them from the original signals. $x(t)$, $d(t)$, and $e(t)$ denote the physical reference, disturbance, and error signals, respectively. P and S represent the primary and secondary paths. F_x, F_e, and F_R represent the reference signal anti-aliasing filter, the error signal anti-aliasing filter, and the reconstruction filter, respectively. $x'[n]$ and $e'[n]$ are the sampled and low-pass filtered reference and error signals, filtered by F_x and F_e, respectively, with $t = nh$, h being the sample time. W_a and W_d represent the analog and digital adaptive feedforward filters. $u(t)$ denotes the control signal, which is the ADAF output, and it is the sum of $u(t) = u_a(t) + u_d(t)$, where $u_a(t)$ is the output of the analog filter and $u_d(t)$ is the reconstructed output of the

Authorized licensed use limited to: UNIVERSITY OF SOUTHAMPTON. Downloaded on January 10,2024 at 08:26:16 UTC from IEEE Xplore. Restrictions apply.
© 2024 IEEE. Personal use is permitted, but republication/redistribution requires IEEE permission. See https://www.ieee.org/publications/rights/index.html for more information.

This article has been accepted for publication in IEEE/ACM Transactions on Audio, Speech and Language Processing. This is the author's version which has not been fully edited and content may change prior to final publication. Citation information: DOI 10.1109/TASLP.2024.3350882

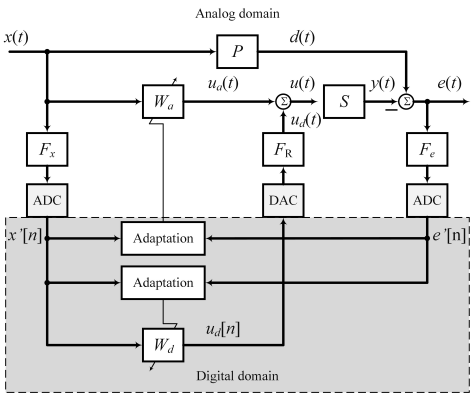

Fig. 2. Block diagram of a parallel analog and digital adaptive controller. Fx and Fe denote the anti-aliasing filters used for the sampling of the reference and error signals, and Fr denotes the reconstruction filter.

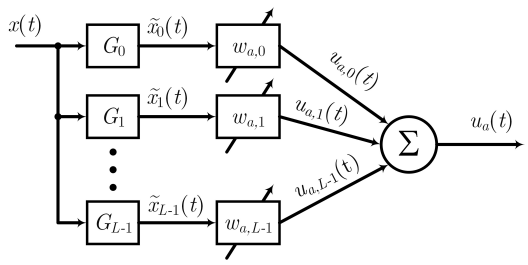

Fig. 3. Block diagram of an analog adaptable state-filtered linear combiner.

digital filter after filtering it with F_R, and $y(t)$ is the control action at the error location.

1) Adaptation of the digital filter: The digital feedforward filter considered here is an FIR filter with K taps, and its input-output relation is given by:

$$u_d[n] = W_d[z] * x'[n] = \sum_{k=0}^{K-1} w_{d,k} x'[n-k], \tag{1}$$

where $*$ denotes the convolution operator, and $W_d[z] = \sum_{k=0}^{K-1} w_{d,k} z^{-k}$. The normalized FxLMS (NFxLMS) method can be used to update the digital filter weights, $w_{d,k}$, at each iteration:

$$w_{d,k}[n+1] = w_{d,k}[n] + \mu_d[n] r'[n-k] e'[n], \tag{2}$$

where

$$\mu_d[n] = \frac{\beta_d}{\sum_{k=0}^{K-1} r'[n-k]^2 + \varepsilon_d}, \tag{3}$$

denotes the normalized adaptation gain, for a positive constant step-size $0 < \beta_d$, and a small positive constant, ε_d, that is added to ensure finite adaptation gains. $r'[n] = \hat{S}'[z] * x'[n]$ in (2) is the sampled filtered reference that is obtained from the convolution of the sampled reference signal $x'[n]$ with the model of the sampled secondary path $\hat{S}'$ that combines the model of the physical analog secondary path with the sampling effects of the reconstruction and the error anti-aliasing filters, ADC, and DAC.

2) Adaptation of the analog filter: An analog adaptable state-filtered linear combiner with L states is considered for the analog filter, as the one shown in Fig. 3, where $G_l(s), l = 0, 1, \ldots, L-1$ denotes the state filters, $\tilde{x}_l$ the lth filtered state reference, $w_{a,l}$ are the adaptable gains, and $u_{a,l}$ are the states' control signals. The analog filter input-output relation is given by:

$$u_a(t) = \sum_{l=0}^{L-1} w_{a,l}(t) \left(G_l(s) * x(t) \right). \tag{4}$$

The state filters are chosen as a 2nd order all-pass filters [29], each tuned based on the Padé approximation for the required delay τ_l:

$$G_l(s) = \frac{1}{4} \frac{s^2 - 6\tau_l^{-1} s + 12\tau_l^{-1}}{s^2 + 6\tau_l^{-1} s + 12\tau_l^{-1}} \approx \frac{1}{4} e^{-\tau_l s}, \tag{5}$$

and $G_0(s) = 1$, such that $\tilde{x}_0(t) = x(t)$ is the direct analog feedthrough signal.

The adaptation of w_l is in the spirit of the original derivation of the FxLMS [4], [20]. Here, the normalized projection algorithm is used [31], [32], and the adaptation law in continuous time is given by:

$$\dot{w}_l(t) = \gamma(t) e(t) r_l(t), \tag{6}$$

where

$$\gamma(t) = \frac{\alpha}{\sum_{l=0}^{L-1} r_l(t)^2 + 1}, \tag{7}$$

denotes the normalized adaptation gain for a positive constant $\alpha > 0$. In (6), $e(t)$ denotes the error signal, and r_l the l filtered state, given by $r_l(t) = \hat{S}(s) * G_l(s) * x(t)$,where $\hat{S}$ is the model of the physical analog secondary path.

A major limitation in implementing the normalized projection is the need to filter the continuous states with the secondary path model, $\hat{S}$, to obtain the filtered state r_l. Therefore, a sampled version of the adaptation is used, which is found to be equivalent to the NFxLMS. By denoting $w_l[n]$ the value of the state gain at time $t = nh$, and assuming that it remains constant between consecutive samples, the solution of the adaptation ODE of (6) is given by:

$$w_l(t) = w_l[n] + \int_{nh}^{t} \gamma(\tilde{t}) e(\tilde{t}) r_l(\tilde{t}) d\tilde{t}, \; n < t/h \leq n+1. \tag{8}$$

And for the consecutive sample time $t = (n+1)h$ one obtains

$$w_l[n+1] = w_l[n] + \int_{nh}^{(n+1)h} \gamma(\tilde{t}) e(\tilde{t}) r_l(\tilde{t}) d\tilde{t}. \tag{9}$$

Thus a recursive adaptation law can be obtained with reasonable accuracy by estimating the integral value between two consecutive sampling times. Assuming zero-order hold, i.e., the signals are constants between sample time, yields the following approximation:

$$\int_{nh}^{(n+1)h} \gamma(\tilde{t}) e(\tilde{t}) r_l(\tilde{t}) d\tilde{t} \approx \mu_a[n] e[n] r_l[n], \tag{10}$$

where $\mu_a[n] = h\gamma[n]$ can be obtained using the normalization law of (3), with a small positive regularization factor in the

Authorized licensed use limited to: UNIVERSITY OF SOUTHAMPTON. Downloaded on January 10,2024 at 08:26:16 UTC from IEEE Xplore. Restrictions apply.
© 2024 IEEE. Personal use is permitted, but republication/redistribution requires IEEE permission. See https://www.ieee.org/publications/rights/index.html for more information.

This article has been accepted for publication in IEEE/ACM Transactions on Audio, Speech and Language Processing. This is the author's version which has not been fully edited and content may change prior to final publication. Citation information: DOI 10.1109/TASLP.2024.3350882

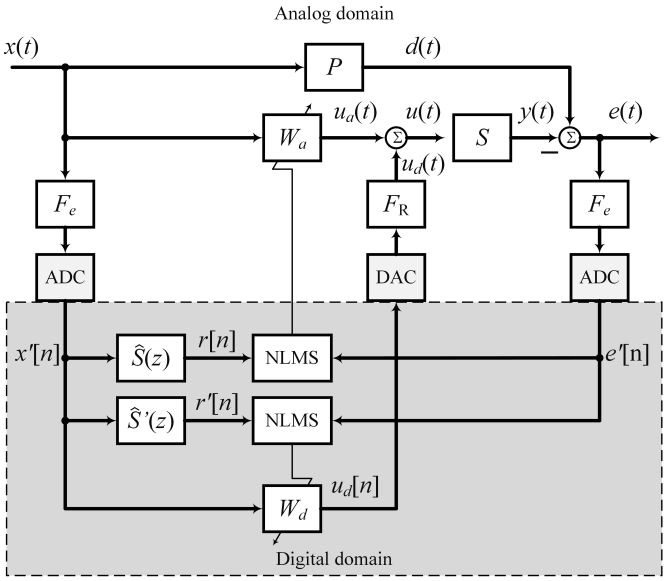

Fig. 4. Block-diagram of the ADAF using NFxLMS adaptation laws for the analog and digital controllers.

denominator of ε_a. The filtered-reference signal used in this adaptation law can be computed digitally as $r_l[n] = \hat{S}[z] * G_l[z] * x[n]$, where $\hat{S}[z] = \mathscr{Z}\left\{\mathscr{L}^{-1}\left\{S(s)\right\}\right\}$ is the sampled-time model of the analog secondary path $S(s)$, and $G_l[z]$ is the sampled-time state filter. If the analog state-filter delay times τ_l are all chosen as integer multiplication of the sample time, then $\tau_l = c_l h$, $c_l \in \mathbb{N}$. In that case, since $G_l(s)$ was designed to mimic discrete delays, its sampled counterpart can be modeled as pure delay, i.e., $G_l[z] = b_l z^{-c_l}$, for $b_0 = 1$, and $b_l = 1/4$ for $l = 1, 2, \ldots, L-1$. The recursive adaptation law is the same as the NFxLMS:

$$w_l[n+1] = w_l[n] + b_l \mu_a[n] e[n] b_l r[n - c_l], \qquad (11)$$

where $r[n] = \hat{S}[z] * x[n]$.

In reality, anti-aliasing filters must be used before the ADC to obtain $e[n]$ and $x[n]$ used in the adaptation law of (11). However, unlike the sampled version, the analog error path does not contain the reconstruction filter. The anti-aliasing filters used to filter both signals can have the same response, since doing so also accommodates the presence of the anti-aliasing filter in the error signal used for the filter adaptation and ensures that the same phase delay is added to the sampled reference and sampled error signals.

The block diagram presented in Fig. 4 shows the proposed adaptation for both the analog and the sampled filters used in the ADAF.

III. Real-time implementation

The performance of ANC headphones depends on the direction of the incident sound field [1], [30]. This can be attributed to the causality of the controller [33], meaning that the delay of the overall secondary path from the reference microphone, via the controller and the loudspeaker, to the error microphone must not be longer than the delay of the primary path from the reference sensor to the error sensor. The ADAF controller proposed here aims to minimize the latency associated with the controller and, by doing so, ensure that the causality is maintained. The customized headphones were placed on a dummy head as in Fig. 1(a), and the reference and error microphones of the left ear cup were measured, the speaker at the left ear cup was used as the secondary source, and a Genelec 8020D loudspeaker was used to generate the primary noise field. A Kemo VBF17J variable filter was used for the anti-aliasing and reconstruction filters, a Yamaha MLA8 mic line amplifier was used for the microphones, and an LD HPA4 amplifier for the headphones' speaker. The anti-aliasing filters were chosen to be the same, as suggested in Section II-B, as low-pass filters with bandwidths of 1 kHz, and the reconstruction as a low-pass filter with a bandwidth of 1.6 kHz. A dSPACE DS1103 controller was used to measure the signals and to implement the digital filter and both adaptation algorithms. A sample rate of 10 kHz was used, which gives a sample time of $h = 0.1$ milliseconds.

A. Design of analog filters

In this section, the design of the prototype analog circuits required for the ADAF controller is described. In the current experiments, only two states were considered for the analog filter. The direct feedthrough and a state that aims at approximating a delay of $3h$ which was chosen since the overall delay of the digital controller was estimated at about $7h$. To obtain the delayed analog state, an all-pass filter was designed based on the RC-opamp circuit of Fig. 5 with a TI μA741 general-purpose operational amplifiers, 2 capacitors with the same capacitance value $\mathrm{C} = 474$ nF, and 4 potentiometers that were tuned to the following resistance values: $\mathrm{R}_1 = \mathrm{R}_3 = 157.5$, $\mathrm{R}_2 = 210$, $\mathrm{R}_4 = 52.5\Omega$. Each of the states was passed via a Maxim Integrated MAX5481 10-bit programmable voltage-divider, controlled by the dSPACE in its up/down digital interface. The two analog channels and the digital filter output were then summed using an inverted summing amplifier with a TI μA741 op-amp and resistors values of $\mathrm{R}_{a0} = 3.9$, $\mathrm{R}_{a1} = \mathrm{R}_d = \mathrm{R}_f = 1\mathrm{M}\Omega$, such that its output is given by:

$$u(t) = -\left(\frac{\mathrm{R}_{a0}}{\mathrm{R}_f} u_{a0}(t) + u_{a1}(t) + u_d(t)\right), \qquad (12)$$

where $u_{a0} = \frac{a_0}{1023} x(t)$ and $u_{a1} = \frac{a_1}{1023} G_1(s) * x(t)$ are the analog control signals associated with the direct feedthrough and the first filtered analog state, $a_0, a_1 = 0, 1, \ldots, 1023$ are the values of each of the voltage dividers, and $u_s(t)$ is the output of the digital control filter pass via the reconstruction filter. The gain of $R_{a0}/R_f = 1/3.9$ was used for u_{a0} to have a similar resolution to both the analog filter states since the steady-state gain of $G_1(s)$ is $G_1(0) = R_4/R_2 = 1/4$. More integrated and elegant designs of analog filters with adaptable gains can be envisaged for a commercial system, but the aim here was to demonstrate the principle of the ADAF.

B. Impulse response estimation

A preliminary experiment was carried out to estimate the impulse responses of the analog secondary path from the

Authorized licensed use limited to: UNIVERSITY OF SOUTHAMPTON. Downloaded on January 10,2024 at 08:26:16 UTC from IEEE Xplore. Restrictions apply.
© 2024 IEEE. Personal use is permitted, but republication/redistribution requires IEEE permission. See https://www.ieee.org/publications/rights/index.html for more information.

This article has been accepted for publication in IEEE/ACM Transactions on Audio, Speech and Language Processing. This is the author's version which has not been fully edited and content may change prior to final publication. Citation information: DOI 10.1109/TASLP.2024.3350882

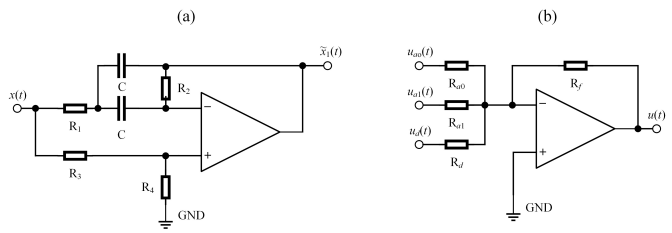

Fig. 5. Electrical component diagram of the all-pass filter (a) and inverting summing amplifier (b) used for the analog filter.

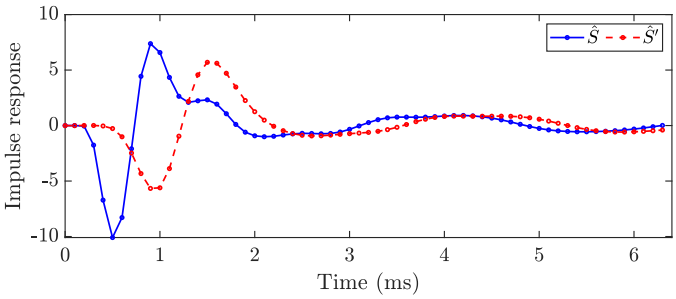

Fig. 6. The measured finite impulse responses of the secondary paths required for the ADAF algorithm. $\hat{S}$ denotes the physical analog secondary path, and $\hat{S}'$ the sampled secondary path.

loudspeaker to the error microphone and the sampled secondary path that includes the filters and sampling delays. The headphone left loudspeaker was excited with a bandlimited noise with a bandpass between 20-2000 Hz. Both systems were modeled as FIR filters with 64 taps, and their impulse responses were fitted using a normalized LMS algorithm. The impulse responses of the low-pass filters used as the anti-aliasing and reconstruction filters, the analog state filter, and the inverting summing amplifier were also estimated using a similar procedure. Fig. 6 shows the measured secondary paths. In Fig. 6, $\hat{S}$ is the identified impulse response of the physical analog secondary path required for the analog filter adaptation, and $\hat{S}'$ is the sampled secondary path, which includes the anti-aliasing and reconstruction filters, that is needed for the adaptation of the digital filter.

The measured response of the analog state filter is shown in Fig. 7(a), its magnitude spectrum, $|G_l(2\pi f)|$, is shown in Fig. 7(b), and its group delay, defined as

$$\tau_{gl}(\omega) = -\frac{dG_l(\omega)}{d\omega}, \tag{13}$$

is shown in Fig. 7(c). It is noted that the magnitude spectrum of Fig. 7(b) is constant at around 0.25, up to 1700 Hz and that the group delay of Fig. 7(c) is also nearly constant up to 800 Hz. The measured group delay in that frequency range is slightly below the design target of $3h$, i.e. 0.3 milliseconds, due to the tolerances of the analog components. The frequency bandwidth of the delay element approximation affects the obtainable bandwidth of the analog control filter. The fact that the group delay at the passband is not exactly equal to an integer product of the sample rate can also affect the overall performance. However, no further attempts were made

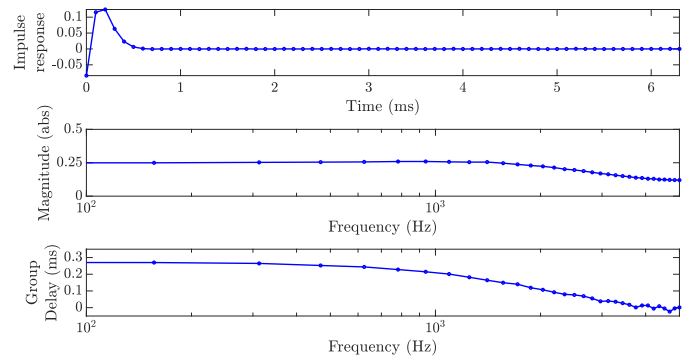

Fig. 7. The measured impulse response (a), magnitude spectrum (b), and group delay (c) of the analog state filter, $G_1(s)$

to minimize these effects here since it was desired to test the proposed ADAF algorithm as is.

C. Anecohic chamber experiments

The performance of the proposed ADAF controller was then tested in the anechoic chamber at the Institute of Sound and Vibration Research. The Genelec speaker was used to excite the primary noise and was moved to several positions around the chamber, always facing the dummy head. Figure 8 shows the three locations that are reported here. Namely, the case where the loudspeaker was placed in front of the dummy head face, where it was placed about $45°$ deg relative to the dummy head, and when it was placed left of the dummy head. These positions are referred to as orientations I, II, and III, respectively.

In these experiments, the analog reference signal was obtained by amplifying the microphone positioned at the outer shell of the left ear cup using the Yamaha MLA8 amplifier, with no additional filtering. Similarly, the sampled reference and error used for the digital controller and for the adaptation were obtained by amplifying the microphones located at the outer and inner shell of the left ear cup, respectively. Both signals were filtered using low-pass filters with 1 kHz bandwidths and then sampled using the dSPACE DS1103 at a rate of 10 kHz. The analog output of the dSPACE DS1103 was first filtered using a low-pass filter with 1.6 kHz bandwidth, then summed with the analog filters' outputs, and amplified using the LD HPA4 before being fed into the left headphone's speaker.

A block-based normalized filtered-reference LMS (BN-FxLMS) was used for the adaptation of the filters, which is based on the NFxLMS proposed in Section II-B. This was done to accommodate the fact that the digitally-controlled voltage dividers used for the analog filter adaptation assume a discrete and finite number of values, and so had a finite resolution, which in this case was comparable to the NFxLMS step size. A buffer of 1 second was used, that contains $N = 10000$ samples of the low-passed filtered reference and error signals. Instead of the adaptation law of (2) and (11), the

Authorized licensed use limited to: UNIVERSITY OF SOUTHAMPTON. Downloaded on January 10,2024 at 08:26:16 UTC from IEEE Xplore. Restrictions apply.
© 2024 IEEE. Personal use is permitted, but republication/redistribution requires IEEE permission. See https://www.ieee.org/publications/rights/index.html for more information.

This article has been accepted for publication in IEEE/ACM Transactions on Audio, Speech and Language Processing. This is the author's version which has not been fully edited and content may change prior to final publication. Citation information: DOI 10.1109/TASLP.2024.3350882

(a)

(b)

(c)

Fig. 8. Experimental setup in the Anechoic chamber for orientations I (a), II (b), and III (c).

BNFxLMS adaptation law was used such that:

$$w_{d,k}[n+1] = w_{d,k}[n] - \sum_{i=0}^{N-K-1} \mu_d[n] r'[n-k-i] e'[n-i], \tag{14}$$

$$w_{a,l}[n+1] = w_{a,l}[n] - \sum_{i=0}^{N-L-1} \mu_a[n] r[n-l-i] e'[n-i], \tag{15}$$

although similar to before, but written here again for completeness, the normalized adaptation gains are given by

$$\mu_d[n] = \frac{\beta d}{\sum_{i=0}^{N-1} r'[n-i]^2 + \varepsilon_d}, \tag{16}$$

$$\mu_a[n] = \frac{\beta a}{\sum_{i=0}^{N-1} r[n-i]^2 + \varepsilon_a}, \tag{17}$$

for small positive ε_d and ε_a, and positive constant step-size β_d and β_a.

The BNFxLMS was used for each of the speaker orientations to adapt a total of five controllers. The five controllers' results will be labeled in the rest of the text as "D" for the case when only the digital controller W_d is used, "A" when only the analog controller W_a is used, "$D + a_0$" when the 0th analog state, or analog feedthrough, is used with the digital controller $W_d + w_{a,0}$, similarly "$D + a_1$" when the 1st analog state, or filtered analog reference signal, $W_d + w_{a,1}$, finally "$ADAF$" when both W_d and both stated of W_a are used.

The constants of (16) and (17) were set as: $\beta_d = 0.025$, $\beta_a = 50$, and $\varepsilon_d = \varepsilon_a = 0.01$. The product of the analog controller adaptation step size and the voltage divider resolution is the adaptation gain for the analog weights, such that $\beta_{a,\mathbf{eff}} = \beta_a \Delta V = 50/1024 = 0.0488$. Therefore the two step-sizes of both controllers are of the same order of magnitude.

The primary noise was generated by passing a white noise via a bandpass filter with a passband between 70-600 Hz, stopbands below 50 Hz and above 1000 Hz, and stopbands' attenuations of 60 dB. Each controller was adapted from zero initial conditions for 200 seconds to obtain the steady-state controller. Each controller was then tested for 30 seconds using a new realization of the generated noise with similar properties.

Figure 9 presents the magnitude levels in the frequency domain of the disturbance and the residual error for each of the steady-state controllers for a chosen reference level. The measured spectrums were obtained by using Welch's method with a Hamming window of 2500 samples, equivalent to 0.25 seconds, and 50% overlap. It is noted that except for when only the analog controller, A, is used, all controllers obtain significant attenuation between 120–560 Hz. Between 560–670 Hz, the D and $D+a_1$ controller magnitude is above that of the ANC off case for orientation I, but their magnitude at these frequencies remains low relative to the peak noise magnitude. Above 670 Hz, some amplification levels are observed for all controllers and in all three orientations. However, this is inside the noise bandpass transition zones, and as seen, the controllers' magnitudes at these frequencies are smaller compared to their magnitudes in the noise passband between 100–600 Hz.

Overall, in the noise passband, the performance of the $D + a_1$ and $ADAF$ is superior to that of the other controllers for all three cases. Not much difference can be seen between the two best controllers. The next best controller seems to be the $D + a_0$. This is mainly notable for Orientation I, when the primary noise delay is the shortest. Based solely on the results of Fig. 9, it is hard to make any quantitative or qualitative assessment of the differences between the three orientations.

Table I report the steady-state noise reduction (NR) of each controller at each orientation between 20–2000 Hz in dB. Based on Table I, it is verified that the largest NR is obtained for orientation III, as expected from the theory. When comparing the obtained NR of each controller for the three orientations, it is noted that while D, $D + a_1$, and $ADAF$ controllers' NRs do become better as the speaker is oriented towards the left of the dummy head, the A and $D + a_0$ controllers' NR does not. A similar pattern is seen in both cases, where the NR of orientation II is the smallest, and the NR of orientation I is the biggest. Finally, for orientations I and II, no clear preference is noted between $D + a_1$ and the $ADAF$ controllers. However, for orientation III, the $D + a_1$ NR is about 1 dB larger than that of the $ADAF$. This is thought to be due to the finite resolution around zero of the voltage dividers.

Authorized licensed use limited to: UNIVERSITY OF SOUTHAMPTON. Downloaded on January 10,2024 at 08:26:16 UTC from IEEE Xplore. Restrictions apply.
© 2024 IEEE. Personal use is permitted, but republication/redistribution requires IEEE permission. See https://www.ieee.org/publications/rights/index.html for more information.

This article has been accepted for publication in IEEE/ACM Transactions on Audio, Speech and Language Processing. This is the author's version which has not been fully edited and content may change prior to final publication. Citation information: DOI 10.1109/TASLP.2024.3350882

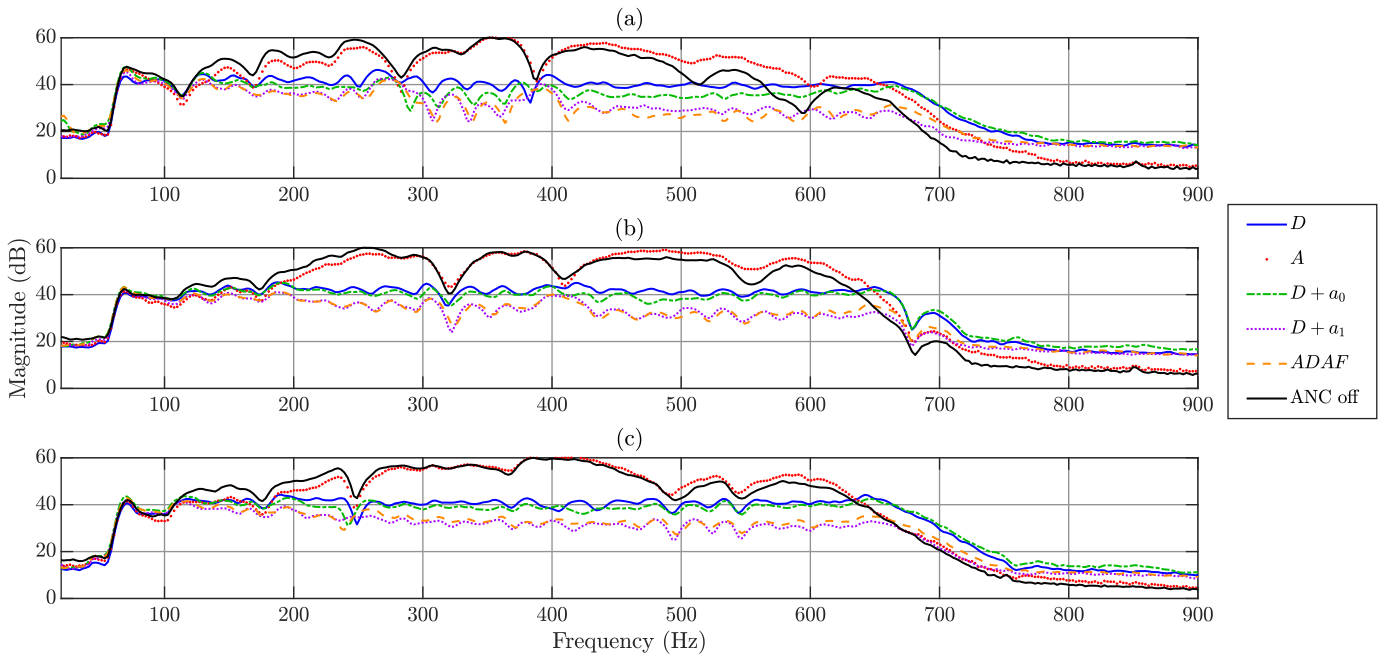

Fig. 9. Steady-state spectral levels for the measured disturbance and residuals error for the five steady-state controllers for orientations I (a), II (b), and III (c). In the legend, D stands for the case when only the digital controller is used, A when only the analog controller is used, $D + a_0$ when the digital controller and the analog feedthrough are both used, $D + a_1$ when the digital controller and the filtered analog signal are used, $ADAF$ when both the digital, analog feedthrough, and filtered analog signal are used, and ANC off is the normalized disturbance when no control is applied.

TABLE I
NOISE REDUCTION IN DB BETWEEN 20–2000 HZ FOR THE THREE ORIENTATIONS AND STEADY-STATE CONTROLLERS.

	D	A	$D + a_0$	$D + a_1$	$ADAF$
Orientation I	11.3	0	13.5	16.3	16.4
Orientation II	11.6	-0.5	12.8	17.4	17.2
Orientation III	12.2	-0.3	13.3	18.6	17.6

D. Controllers' filter impulse responses

The continuous time steady-state impulse response of each of the controllers was computed as

$$w(t) = -\left(\frac{1}{3.9} w_{a,0} g_0(t) + w_{a,1} g_1(t) + R(s) * w_d(t)\right) \tag{18}$$

where $w_d(t) = w_{d,k}$, $kh \leq t < (k+1)h$, $g_0(t) = \delta(t)$, $g_1(t)$ is the estimated impulse response of the state filter, $G_1(s)$, shown in Fig. 7, and $R(s)$ is the identified model of the reconstruction filter, which was identified using the procedure described in Section III-B. The Wiener filter controller was also fitted offline, using the measured reference and disturbance signals in the case of no control. However, it was found that the Wiener filter impulse response depends heavily on the choice of regularization factor and so was not used in the comparison.

Figure 10 shows the continuous-time impulse response of the different steady-state controllers for the three orientations. The impulse response of the analog controller is not shown since it performs badly. For each orientation, the longer-term response is also shown in the enlargement. From the initial transient of the impulse responses, it is noted that the impulse response of the purely digital controller, D, is relatively small in absolute values compared to the other impulse responses. The $D + a_1$ and $ADAF$ controllers' impulse responses are smooth. But while the $ADAF$ and $D + a_0$ initial values are negative, the $D + a_1$ initial value is positive. The $D + a_0$ transient response is then comparable in its magnitude to that of the D transient response. The positive initial value seen for the $D + a_1$ is due to the undershot of the state-filter $g_1(t)$ seen in Fig. 7(a). The impulse responses of the $D+a_1$ and $ADAF$ controllers are very similar after about 0.1 milliseconds, reflecting their similar performance in Table I.

IV. DISCUSSION AND CONCLUSIONS

A parallel adaptable digital and analog filter (ADAF) was considered for ANC in a headphone application. The analog filter is based on an adaptable state-filter linear combiner. An analog all-pass filter was designed using an RC-amp circuit as the state-filter to approximate the desired analog delay. By choosing the state-filter delay time to be equal to an integer product of the base sample time, the NFxLMS can be used for the analog weights adaptations, although it was shown that in practice this assumption is not critical.

A two states analog controller was designed and its variable gains were implemented using 10-bit linear voltage dividers that were controlled using a dSPACE RTI platform. A preliminary experiment was carried out to identify the physical analog secondary path and the sampled secondary path required for the filters' adaptation. In this work, the state filter, anti-aliasing filter, and reconstruction filter impulse responses were also identified. However, this is not necessary for the proposed

Authorized licensed use limited to: UNIVERSITY OF SOUTHAMPTON. Downloaded on January 10,2024 at 08:26:16 UTC from IEEE Xplore. Restrictions apply.
© 2024 IEEE. Personal use is permitted, but republication/redistribution requires IEEE permission. See https://www.ieee.org/publications/rights/index.html for more information.

This article has been accepted for publication in IEEE/ACM Transactions on Audio, Speech and Language Processing. This is the author's version which has not been fully edited and content may change prior to final publication. Citation information: DOI 10.1109/TASLP.2024.3350882

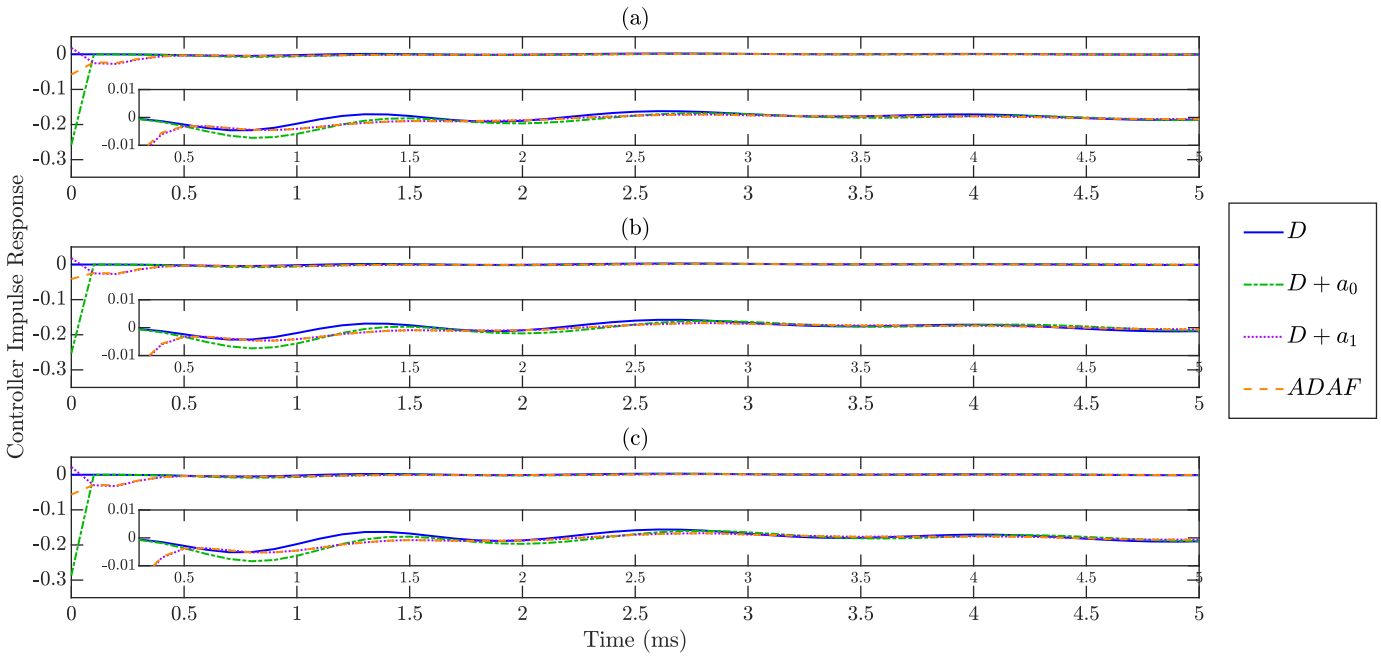

Fig. 10. Impulse responses of the steady-state controllers for orientations I (a), II (b), and III (c). Due to the large values at the initial time, the enlargement of each subplot shows the zoomed-in responses at times above 0.3 ms. In the legend, D stands for the case when only the digital controller is used, $D + a_0$ when the digital controller and the analog feedthrough are both used, $D + a_1$ when the digital controller and the filtered analog signal are used, and $ADAF$ when both the digital, analog feedthrough, and filtered analog controllers are used.

adaptation algorithm but was done only to enable a better understanding of the results.

Next, the ADAF performance was tested in an anechoic chamber for different orientations of the primary noise source. It was verified that the digital controller performance depends on the direction of the primary noise. Moreover, for all orientations, the addition of any of the analog elements considered, the direct feedthrough, the first state filter with an approximately 0.3 milliseconds delay, or both, improve the overall noise reduction compared to using only the digital one. While the addition of only the direct feedthrough improves the NR by about 1 or 2 dB and is most affective when the noise source was placed directly in front of the dummy head, the use of the analog state filter contributes to an increase in the NR of about 5 to 6 dB regardless of the orientation. No additional improvement was seen when using both analog states compared to only using the first analog state-filter.

The continuous-time impulse responses of all steady-state controllers were compared. When only the first state-filter was used, a positive initial value was seen, unlike all the other controllers' initial values, which were negative. The sign change of the initial value is due to the negative initial value of the 2nd-order all-pass filter used in the approximation of the required delay. A higher-order state-filter could be designed using either the Padé or a least-squares Equiripple approximation to minimize the undershot.

Conventionally, the processing delay in active control systems is reduced by using a very fast sample rate, which increases the computational effort and can lead to numerical ill-conditioning and misadjustment. The theoretical observations and experimental results here show that it can be advantageous to not only include an adaptable analog feedthrough path in a sampled implementation but also to include additional analog state-filters.

Acknowledgment

The authors would like to thank Ian Stothers for fruitful discussions and exchange of ideas.

References

[1] B. Rafaely and M. Jones, "Combined feedback–feedforward active noise-reducing headset—the effect of the acoustics on broadband performance," *The Journal of the Acoustical Society of America*, vol. 112, no. 3, pp. 981–989, 2002.

[2] T. Bowe, "What are hybrid noise-canceling headphones?" 2019. [Online]. Available: https://www.gearpatrol.com/tech/audio/a594566/hybrid-noise-canceling-headphones/

[3] "Anc headsets aren't all the same: The three types of anc," Jabra GN.

[4] D. Morgan, "An analysis of multiple correlation cancellation loops with a filter in the auxiliary path," *IEEE Transactions on Acoustics, Speech, and Signal Processing*, vol. 28, no. 4, pp. 454–467, 1980.

[5] J. C. Burgess, "Active adaptive sound control in a duct: A computer simulation," *The Journal of the Acoustical Society of America*, vol. 70, no. 3, pp. 715–726, 1981.

[6] B. Widrow and S. D. Stearns, *Adaptive signal processing*. Prentice-Hall Englewood Cliffs, NJ, 1985.

[7] S. M. Kuo, I. Panahi, K. M. Chung, T. Horner, M. Nadeski, and J. Chyan, "Design of active noise control systems with the tms320 family," *Texas Instruments*, 1996.

[8] S. M. Kuo, S. Mitra, and W.-S. Gan, "Active noise control system for headphone applications," *IEEE Transactions on Control Systems Technology*, vol. 14, no. 2, pp. 331–335, 2006.

[9] C.-Y. Chang and S.-T. Li, "Active noise control in headsets by using a low-cost microcontroller," *IEEE Transactions on industrial electronics*, vol. 58, no. 5, pp. 1936–1942, 2010.

[10] K.-K. Shyu, C.-Y. Ho, and C.-Y. Chang, "A study on using microcontroller to design active noise control systems," in *2014 IEEE Asia Pacific Conference on Circuits and Systems (APCCAS)*. IEEE, 2014, pp. 443–446.

Authorized licensed use limited to: UNIVERSITY OF SOUTHAMPTON. Downloaded on January 10,2024 at 08:26:16 UTC from IEEE Xplore. Restrictions apply.
© 2024 IEEE. Personal use is permitted, but republication/redistribution requires IEEE permission. See https://www.ieee.org/publications/rights/index.html for more information.

This article has been accepted for publication in IEEE/ACM Transactions on Audio, Speech and Language Processing. This is the author's version which has not been fully edited and content may change prior to final publication. Citation information: DOI 10.1109/TASLP.2024.3350882

[11] H.-S. Vu and K.-H. Chen, "A low-power broad-bandwidth noise cancellation vlsi circuit design for in-ear headphones," *IEEE Transactions on Very Large Scale Integration (VLSI) Systems*, vol. 24, no. 6, pp. 2013–2025, 2015.

[12] M. Bahoura and H. Ezzaidi, "Fpga-implementation of parallel and sequential architectures for adaptive noise cancelation," *Circuits, Systems, and Signal Processing*, vol. 30, pp. 1521–1548, 2011.

[13] D. Shi, C. Shi, and W.-S. Gan, "A systolic fxlms structure for implementation of feedforward active noise control on fpga," in *2016 Asia-Pacific Signal and Information Processing Association Annual Summit and Conference (APSIPA)*. IEEE, 2016, pp. 1–6.

[14] S. Elliott, *Signal processing for active control*. Elsevier, 2000.

[15] S. Liebich, J. Fabry, P. Jax, and P. Vary, "Signal processing challenges for active noise cancellation headphones," in *Speech Communication; 13th ITG-Symposium*. VDE, 2018, pp. 1–5.

[16] B. Lam, W.-S. Gan, D. Shi, M. Nishimura, and S. Elliott, "Ten questions concerning active noise control in the built environment," *Building and Environment*, vol. 200, p. 107928, 2021.

[17] M. R. Bai, Y. Lin, and J. Lai, "Reduction of electronic delay in active noise control systems—a multirate signal processing approach," *The Journal of the Acoustical Society of America*, vol. 111, no. 2, pp. 916–924, 2002.

[18] Z. Zhang, M. Wu, L. Yin, C. Gong, J. Wang, S. Zhou, and J. Yang, "Robust feedback controller combined with the remote microphone method for broadband active noise control in headrest," *Applied Acoustics*, vol. 195, p. 108815, 2022.

[19] V. Patel, S. S. Bhattacharjee, J. Cheer, and N. V. George, "Hybrid feedback active noise control headset based on binaural signal utilization," *Applied Acoustics*, vol. 200, p. 109062, 2022.

[20] D. Morgan and S. Craig, "Real-time adaptive linear prediction using the least mean square gradient algorithm," *IEEE Transactions on Acoustics, Speech, and Signal Processing*, vol. 24, no. 6, pp. 494–507, 1976.

[21] A. C. Carusone and D. A. Johns, "Digital lms adaptation of analog filters without gradient information," *IEEE Transactions on Circuits and Systems II: Analog and Digital Signal Processing*, vol. 50, no. 9, pp. 539–552, 2003.

[22] I. Stothers and I. Scott, "Adaptive control unit with feedback compensation," U.S. Patent US20 070 098 119A1, may 3, 2007.

[23] D. Tinker, "Apparatus and methods for an acoustic noise cancellation audio headset," U.S. Patent US11 393 446B2, Jul. 19, 2022.

[24] S. Karni and G. Zeng, "The analysis of the continuous-time lms algorithm," *IEEE Transactions on Acoustics, Speech, and Signal Processing*, vol. 37, no. 4, pp. 595–597, 1989.

[25] A. J. Velosoa and V. H. Nascimentob, "Headphone with active noise control using analog adaptive filters," in *inter-noise Environmental Noise Control, The 2005 Congress and Exposition on Noise Control Engineering*. Citeseer, 2005.

[26] D. A. Johns, W. M. Snelgrove, and A. S. Sedra, "Continuous-time lms adaptive recursive filters," *IEEE Transactions on Circuits and Systems*, vol. 38, no. 7, pp. 769–778, 1991.

[27] A. Carusone and D. Johns, "Analogue adaptive filters: past and present," *IEE Proceedings Circuits Devices and Systems*, vol. 147, no. 1, pp. 82–90, 2000.

[28] R. Piche, "Low-order rational all-pass approximations to es," *IFAC Proceedings Volumes*, vol. 23, no. 8, pp. 183–186, 1990.

[29] Y. Vered and S. J. Elliott, "Adaptive analog and digital active noise control," in *Inter-Noise and Noise-Con Congress and Conference Proceedings*. Institute of Noise Control Engineering, 2023.

[30] J. Cheer, V. Patel, and S. Fontana, "The application of a multi-reference control strategy to noise cancelling headphones," *The Journal of the Acoustical Society of America*, vol. 145, no. 5, pp. 3095–3103, 2019.

[31] P. A. Ioannou and J. Sun, *Robust adaptive control*. PTR Prentice-Hall Upper Saddle River, NJ, 1996, vol. 1.

[32] K. J. Åström and B. Wittenmark, *Adaptive control*. Courier Corporation, 2013.

[33] L. Zhang and X. Qiu, "Causality study on a feedforward active noise control headset with different noise coming directions in free field," *Applied Acoustics*, vol. 80, pp. 36–44, 2014.

Yoav Vered Yoav vered received his B.Sc. (2016, Summa cum Laude), Master (2017), and PhD (2021) at the Mechanical Engineering faculty at Technion-Israel Institute of Technology. His PhD dissertation dealt with the analytical and numerical modelling of finite-length fluid-filled coupled waveguides and the development of experimental methodologies to identify and control the dispersive nature of such waveguides.

Currently, Dr Vered is a Research Fellow at the Institute of Sound and Vibration Research at the University of Southampton as part of the DigiTwin project. His postdoctoral research focuses on robust and reconfigurable control for active noise and vibration control of nonautonomous and nonlinear dynamical systems. His research interests include physics-inspired modelling of sound and vibration phenomena and active and adaptive feedback control of time-varying and nonlinear systems.

Stephen Elliott Steve Elliott graduated with first class joint honours in physics and electronics from the University of London, in 1976, and received his PhD from the University of Surrey in 1979 for a dissertation on musical acoustics.

He was appointed Lecturer at the Institute of Sound and Vibration Research (ISVR), University of Southampton, in 1982, was made Senior Lecturer in 1988, Professor in 1994, and served as Director of the ISVR from 2005 to 2010. His research interests have been mostly concerned with the connections between the physical world, signal processing and control, mainly in relation the active control of sound using adaptive filters and the active feedback control of vibration. This work has resulted in the practical demonstration of active control in propeller aircraft, cars and helicopters. His current research interests include modular systems for active feedback control and modelling the active processes within the cochlear.

Professor Elliott has published over 300 papers in refereed journals and 600 conference papers and is co-author of Active Control of Sound (with P A Nelson 1992), Active Control of Vibration (with C R Fuller and P A Nelson 1996) and author of Signal Processing for Active Control (2001). He is a Fellow of the Acoustical Society of America, was jointly awarded the Tyndall Medal from the Institute of Acoustics in 1992 and the Kenneth Harris James Prize from the Institution of Mechanical Engineers in 2000.

He was made a Fellow of the Royal Academy of Engineering in 2009

Authorized licensed use limited to: UNIVERSITY OF SOUTHAMPTON. Downloaded on January 10,2024 at 08:26:16 UTC from IEEE Xplore. Restrictions apply.
© 2024 IEEE. Personal use is permitted, but republication/redistribution requires IEEE permission. See https://www.ieee.org/publications/rights/index.html for more information.